JOURNAL OF GUIDANCE, CONTROL, AND DYNAMICS
Vol. 24, No. 2, March–April 2001

Optimization of Launch Vehicle Ascent Trajectories with Path Constraints and Coast Arcs

Peter F. Gath* and Anthony J. Calise†
Georgia Institute of Technology, Atlanta, Georgia 30332-0150

This paper describes improvements made to a hybrid analytic/numerical algorithm for optimization of launch vehicle trajectories. Modifications are described that improve the accuracy of the solution. In addition, the algorithm has been extended to include path constraints for normal force and angle of attack, and the terminal constraints have been generalized to allow optimal attachment to a target orbit defined by inclination, apogee radius, and perigee radius. Singularities that occur for circular orbits and for equatorial orbits are identified. Finally, necessary conditions are derived and applied for the introduction of coasting arcs that are typically required for a great variety of missions. To verify the algorithm presented in this paper, results of a test mission to a 100-nm circular equatorial orbit have been compared with two other independent optimization codes.

Nomenclature

A = aerodynamic force in axial direction, lbs
A_e = nozzle exit area, ft^2
a = semi-major axis, ft
a_a = axial acceleration, ft/s^2
$a_{\max}$ = maximum axial acceleration, ft/s^2
c_e = nozzle exit velocity, ft/s
E = orbital energy, ft^2/s^2
e = eccentricity
H = Hamiltonian
h = orbital angular momentum, ft^2/s
M = Mach number
m = mass, lb
N = aerodynamic force in normal direction, lbs
$\boldsymbol{P}$ = velocity costate vector/primer vector, s/ft
p_a = atmospheric pressure, lbs/ft^2
$\boldsymbol{p}_V$ = collocation variables for velocity state, ft/s^2
$\boldsymbol{Q}$ = position costate vector, 1/ft
$\boldsymbol{q}_R$ = collocation variables for position costate
$\boldsymbol{q}_V$ = collocation variables for velocity costate
$\boldsymbol{R}$ = radius vector from Earth center, ft
R_e = Earth radius, ft
r_a = apogee radius, ft
r_p = perigee radius, ft
T = thrust, lbs
T_{vac} = maximum available vacuum thrust, lbs
$\boldsymbol{V}$ = inertial velocity vector, ft/s
α = angle of attack, rad
β = angle between final radius and velocity vector, rad
ε = constraint multiplier
λ_m = mass costate, 1/lb
μ = gravitational constant, ft^3/s^2
ω = Schuler frequency, 1/s
$\mathbf{1}_b$ = unity vector along body axis
$\mathbf{1}_f$ = unity vector perpendicular to orbit plane
$\mathbf{1}_N$ = unity vector pointing north
$\mathbf{1}_n$ = unity vector perpendicular to body axis
$\mathbf{1}_P$ = unity vector along primer vector
$\mathbf{1}_R$ = unity vector along radius vector
$\mathbf{1}_V$ = unity vector along velocity vector

Received 3 December 1999; revision received 26 April 2000; accepted for publication 28 April 2000.

*Research Scholar, School of Aerospace Engineering; currently Ph.D. Student, Institute of Flight Mechanics and Control Theory, University of Stuttgart, 70550 Stuttgart, Germany; Peter.Gath@ifr.uni-stuttgart.de. Student Member AIAA.

†Professor, School of Aerospace Engineering; anthony.calise@ae.gatech.edu. Fellow AIAA.

Introduction

ADVANCED launch vehicle design and performance analysis is highly coupled to the trajectory analysis problem of how to guide the vehicle to achieve maximum payload to a desired orbit. The most important factor for cost reduction is a mass-optimal design of the whole mission. Besides improvements of engines and reduction of structural mass by using advanced materials, the ascent trajectory of the launch vehicle has to be optimized with respect to fuel consumption. Another aspect of cost reduction is launching several satellites at once. Therefore, vehicle designs that employ upper stages with a very low thrust/weight ratio are of particular interest.

Traditional launch vehicle guidance has employed open-loop guidance in the atmospheric phase, and closed-loop guidance once the vehicle is sufficiently outside the atmosphere. However, the process of constructing an open-loop solution can be costly, particularly in vehicle synthesis where many optimized profiles may be required before a final design is achieved. There exist a variety of trajectory optimization codes that utilize both direct and indirect methods for optimization. However, all of these codes require a reasonably good starting guess for convergence, and most are not suitable for real-time guidance application.

In Ref. 1, a hybrid analytic/numerical approach is described that offers the potential for efficient online calculation of optimal trajectories. One unique feature is that the method does not require a starting guess. The solution process uses a homotopy method, which starts from a nearly analytic vacuum solution and gradually introduces atmospheric effects until a converged solution is obtained. Once a converged solution from the launch point is available, then subsequent guidance updates can be executed in fractions of a second due to the nearly analytic nature of the solution process.

This paper describes modifications and extensions to the code described in Ref. 1 that greatly enhance its accuracy and usefulness as a trajectory analysis element in a vehicle synthesis code. Path constraints on angle of attack and normal force have been added. The terminal constraints as defined in Ref. 1 are overly restrictive in that they fully define the final orbit plane, and the attachment point is constrained to occur at perigee. Normally, for vehicle synthesis, prescribing as few of the orbital elements as possible is desirable, so that the design is not optimized for too small a spectrum of missions. The new formulation removes constraints on the location of the ascending node and the argument of perigee. The singularities that these new formulations can produce are identified.

In Ref. 1, no provision was made for coasting arcs, which are essential, for example, when launching from northern latitudes and going to an equatorial orbit. The duration of coast arcs is significantly longer than the total duration of burn arcs. Furthermore, the coast arcs occur outside the atmosphere. However, they can significantly impact the optimal path within the atmosphere. Therefore, every effort was made to incorporate known results for analytical solutions

of the state and costate equations and sensitivity analysis needed for optimization.[2,3] This sensitivity analysis enhances both efficiency and accuracy of the solution process. New optimality conditions for the start and end times of coast arcs have been derived. These derivations were necessary because the two-point boundary value problem is treated as a series of fixed burn time problems, compared to the free time problems treated in Refs. 3–6. Included is a condition for determining when the prescribed number of coast arcs is optimal.

The implementation of state and costate propagation during burn phases uses the Schuler frequency referenced to the start of each burn phase, as described in Refs. 4–6. The use of this frequency reduces the corrections needed for the linear gravity model for high altitude orbits. Furthermore, the performance index has been changed to maximize final orbital energy. This change was essential to allow for the introduction of new terminal constraints. Finally, Ref. 1 used the vacuum optimality condition to eliminate the control variable. Here we describe a method for correcting the vacuum solution by using the full optimality condition for the atmospheric portion of the trajectory.

The numerical results presented here are for a vehicle configuration with a very low thrust/weight ratio upper stage. Optimal solutions for these configurations are difficult to converge, particularly with respect to their angle-of-attack profiles.

Analytic Development

Problem Formulation

During burn arcs, the equations of motion for flight in a central gravitational field are expressed in an inertial, Earth-centered coordinate frame as shown in Fig. 1.

$$\begin{bmatrix} \dot{\boldsymbol{V}} \\ \dot{\boldsymbol{R}} \\ \dot{m} \end{bmatrix} = \begin{bmatrix} -\omega^2 \boldsymbol{R} + T_{\text{vac}}/m \cdot \mathbf{1}_p + \boldsymbol{p}_V(t) \\ \boldsymbol{V} \\ -T_{\text{vac}}/c_e \end{bmatrix} \tag{1}$$

where ω is the so-called Schuler frequency defined as

$$\omega = \sqrt{\mu / r_{\text{ref}}^3} \tag{2}$$

The reference radius r_{ref} is the magnitude of the radius vector at the beginning of each burn arc. Earth radius is used as a reference radius for the first burn arc. The collocation variables $\boldsymbol{p}_V(t)$ are calculated as

$$\boldsymbol{p}_V(t) = 1/m \cdot \{T_{\text{vac}} \cdot (\mathbf{1}_b - \mathbf{1}_P) - [A + A_e \cdot p_a(\boldsymbol{R})] \cdot \mathbf{1}_b + N \cdot \mathbf{1}_n\} + \boldsymbol{R} \cdot (\omega^2 - \mu/R^3) \tag{3}$$

As described in Ref. 1, a vacuum solution where the collocation variables are set to zero is generated first. Note from the first element of Eq. (1) that the vacuum solution uses a linear gravity law, which is later corrected by the last term in Eq. (3). Equation (1) also uses the vacuum optimality condition that aligns the thrust vector with the first three components of the costate vector,[3] whereas $\mathbf{1}_b$ in Eq. (3) corresponds to using the full optimality condition (including aerodynamic terms). These approximations permit a nearly analytic solution for the state and costate variables associated with the vacuum solution. The optimization problem is reduced to solving a set of six nonlinear algebraic equations that represent a two-point boundary value problem in which the unknown initial costate values are determined so that the constraints and transversality conditions at final time are met. The collocation variables are initially evaluated along the vacuum solution and are gradually introduced as an additional forcing term to the solution process. This gradual introduction will, of course, change the trajectory profile, so the two-point boundary value solution is repeated, and the collocation variables are recomputed until the process converges.

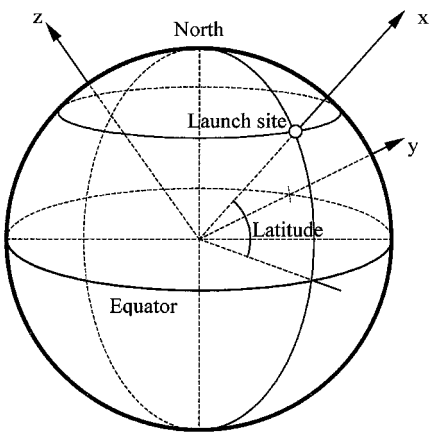

Fig. 1 Coordinate frame.

Coast arcs are assumed to occur outside the atmosphere only. Furthermore, an inverse-square-law gravity field is required in constructing the vacuum trajectory because coast arcs can be of very long duration in comparison to burn arcs and can involve large changes in the radius vector. The equations of motion reduce to

$$\ddot{\boldsymbol{R}} = -\mu/r^3 \cdot \boldsymbol{R} \tag{4}$$

Equations (1–4) can be nondimensionalized using the redefinitions given in Ref. 1. If these are used, all equations remain the same except that $\mu = 1$ in the nondimensional version. In the following, all formulas will be presented in this nondimensional form, but all numerical results will be presented in dimension form.

Using the vacuum optimality condition, Eqs. (1) and (4) can be solved analytically, except for the thrust integrals in Eq. (1). If the collocation variables are assumed to be linear functions of time between nodes, the propagation of the states within burn arcs can then be expressed as

$$\begin{bmatrix} \boldsymbol{R}(\tau) \\ \boldsymbol{V}(\tau) \end{bmatrix} = \Psi \cdot \begin{bmatrix} \boldsymbol{R}_0 \\ \boldsymbol{V}_0 \end{bmatrix} + \Omega \cdot W + \begin{bmatrix} (1/\omega^2)(1 - \cos\omega\tau) \cdot I_3 & (1/\omega^2)[\tau - (1/\omega)\sin\omega\tau] \cdot I_3 \\ (1/\omega)\sin\omega\tau \cdot I_3 & (1/\omega^2)(1 - \cos\omega\tau) \cdot I_3 \end{bmatrix} \times \begin{bmatrix} \boldsymbol{p}_{V,0} \\ \dot{\boldsymbol{p}}_{V,0} \end{bmatrix} \tag{5}$$

where the matrices Ψ, Ω, and W are as shown in Refs. 6 and 7, and I_3 is a 3×3 identity matrix. The time derivative $\dot{\boldsymbol{p}}_{V,0}$ is calculated as

$$\dot{\boldsymbol{p}}_{V,0} = [\boldsymbol{p}_V(\tau) - \boldsymbol{p}_{V,0}]/\tau \tag{6}$$

The analytic solution of Eq. (4) for coast arcs is given in Refs. 2 and 8.

Hamiltonian and Costate Propagation

The Hamiltonian of the system given in Eq. (1) can be expressed in the form

$$H = H_0 + H_{\text{atmos}} + \varepsilon \cdot \text{constraints} \tag{7}$$

where

$$H_0 = \boldsymbol{P}^T \cdot \left(-\omega^2 \boldsymbol{R} + T_{\text{vac}}/m \cdot \mathbf{1}_p\right) + \boldsymbol{Q}^T \cdot \boldsymbol{V} - \lambda_m \cdot T_{\text{vac}}/c_e$$

$$H_{\text{atmos}} = \boldsymbol{P}^T \cdot \boldsymbol{p}_V(t) \tag{8}$$

As shown in Ref. 1, the differential equations for the costates can be written in the following form during burn arcs:

$$\begin{bmatrix} \dot{\boldsymbol{P}} \\ \dot{\boldsymbol{Q}} \end{bmatrix} = \begin{bmatrix} -\boldsymbol{Q} + \boldsymbol{q}_V(t) \\ \omega^2 \boldsymbol{P} - \boldsymbol{q}_R(t) \end{bmatrix}, \qquad \boldsymbol{q}_V(t) = -\frac{\partial H_{\text{atmos}}}{\partial \boldsymbol{V}}$$

$$\boldsymbol{q}_R(t) = \frac{\partial H_{\text{atmos}}}{\partial \boldsymbol{R}} \tag{9}$$

The closed-form solution for the propagation of the costates is given by

$$\begin{bmatrix} \boldsymbol{P}(\tau) \\ -\boldsymbol{Q}(\tau) \end{bmatrix} = \Psi \cdot \begin{bmatrix} \boldsymbol{P}_0 \\ -\boldsymbol{Q}_0 \end{bmatrix} + \begin{bmatrix} (1/\omega)\sin\omega\tau \cdot I_3 & (1/\omega^2)(1-\cos\omega\tau)\cdot I_3 \\ -(1-\cos\omega\tau)\cdot I_3 & -[\tau-(1/\omega)\sin\omega\tau]\cdot I_3 \end{bmatrix} \begin{bmatrix} \boldsymbol{q}_{V,0} \\ \dot{\boldsymbol{q}}_{V,0} \end{bmatrix} + \begin{bmatrix} (1/\omega^2)(1-\cos\omega\tau)\cdot I_3 & (1/\omega^2)[\tau-(1/\omega)\sin\omega\tau]\cdot I_3 \\ (1/\omega)\sin\omega\tau \cdot I_3 & (1/\omega^2)(1-\cos\omega\tau)\cdot I_3 \end{bmatrix} \times \begin{bmatrix} \boldsymbol{q}_{R,0} \\ \dot{\boldsymbol{q}}_{R,0} \end{bmatrix} \tag{10}$$

Equation (10) also treats the collocation variables $\boldsymbol{q}_R(t)$ and $\boldsymbol{q}_V(t)$ as linear functions of time between evaluation nodes. Their time derivatives at t_0 are calculated in a form similar to Eq. (6).

During coast arcs, the costates are expressed as

$$\dot{\boldsymbol{P}} = -\boldsymbol{Q}, \qquad \dot{\boldsymbol{Q}} = (-3\cdot \boldsymbol{R}^T \cdot \boldsymbol{P}/r^5)\cdot \boldsymbol{R} + 1/r^3 \cdot \boldsymbol{P} \tag{11}$$

The closed form solution for the propagation of the costates is given in Refs. 4 and 8.

Performance Index and Terminal Constraints

The problem is treated as a series of fixed final time, two-point boundary value problems. The objective is to maximize orbital energy:

$$\Phi = E_f = \tfrac{1}{2}V_f^2 - 1/R_f \tag{12}$$

Final time is then adjusted so that the desired orbital energy is achieved. This adjustment is equivalent to maximizing the mass (minimizing the fuel consumed) to a specified orbit for free terminal time. The desired final energy can be calculated as $E_{f,d} = -1/(r_a + r_p)$. The final time is adjusted by using the fact that the variation in the performance index due to a variation in final time can be expressed as $\delta J = H(t_f)\cdot \delta t_f$. This leads to the expression

$$\Delta t_f = \frac{\Delta E_f}{H(t_f)} = \frac{-1/(r_a+r_p) - \left(V_f^2/2 - 1/R_f\right)}{-\boldsymbol{P}^T\cdot\boldsymbol{R}/R^3 + |\boldsymbol{P}|\cdot T_{\text{vac}}/m + \boldsymbol{Q}^T\boldsymbol{V}} \tag{13}$$

for the perturbation in final time.

Terminal constraints for attachment at perigee are given in terms of inclination, perigee radius, and flight path angle:

$$\psi_{\text{perigee},1} = \left[\begin{array}{c} \mathbf{1}_N^T \cdot \dfrac{\mathbf{1}_R \times \mathbf{1}_V}{|\mathbf{1}_R \times \mathbf{1}_V|} - \cos(i_d) \\ |\boldsymbol{R}| - r_{p,d} \\ \boldsymbol{R}^T \cdot \boldsymbol{V} \end{array}\right]_{t=t_f} = 0 \tag{14}$$

This formulation is suitable for attachment to both circular and elliptical orbits. For a free attachment point on elliptical orbits, it becomes necessary to replace the last two constraints in Eq. (14) by a single constraint. Several approaches were taken, such as constraining the final momentum or eccentricity. However, the best results were obtained by constraining perigee radius of the target orbit. For this formulation, the terminal constraints can be expressed as

$$\psi_{\text{free},1} = \left[\begin{array}{c} \mathbf{1}_N^T \cdot \dfrac{\mathbf{1}_R \times \mathbf{1}_V}{|\mathbf{1}_R \times \mathbf{1}_V|} - \cos(i_d) \\ \dfrac{1}{2/R - V^2}\left(1 - \sqrt{1 - \left(\dfrac{2}{R} - V^2\right)\cdot |\boldsymbol{R}\times\boldsymbol{V}|^2}\right) - r_{p,d} \end{array}\right]_{t=t_f} = 0 \tag{15}$$

To formulate the two-point boundary value problem, three additional terminal constraints are required for attachment at perigee, and four additional terminal constraints are required when the attachment point is free. These additional constraints are obtained using the transversality conditions, which, in general, have the form

$$\begin{aligned} \boldsymbol{P}_f &= V\cdot \mathbf{1}_V + \nu_1 \cdot \psi_{1V} + \nu_2 \cdot \psi_{2V} + \nu_3 \cdot \psi_{3V} \\ \boldsymbol{Q}_f &= 1/R^2 \cdot \mathbf{1}_R + \nu_1 \cdot \psi_{1R} + \nu_2 \cdot \psi_{2R} + \nu_3 \cdot \psi_{3R} \end{aligned} \tag{16}$$

In the case of an attachment at perigee, we have

$$\psi_{1V} = a_v \cdot \mathbf{1}_f, \qquad \psi_{1R} = -a_R \cdot \mathbf{1}_f, \qquad \psi_{2V} = 0, \qquad \psi_{2R} = \mathbf{1}_R$$

$$\psi_{3V} = \boldsymbol{R}, \qquad \psi_{3R} = \boldsymbol{V}, \qquad a_V = \frac{\mathbf{1}_f^T\cdot(\mathbf{1}_N \times \mathbf{1}_R)}{V\cdot\sin\beta}$$

$$a_R = \frac{\mathbf{1}_f^T\cdot(\mathbf{1}_N \times \mathbf{1}_V)}{R\cdot\sin\beta} \tag{17}$$

One way to eliminate ν_1–ν_3 in Eq. (16) is to form the inner product of Eq. (16) with the vectors $\mathbf{1}_f$, $\mathbf{1}_R$, and $\mathbf{1}_V$. This procedure results in the following additional terminal constraints for attachment at perigee:

$$\psi_{\text{perigee},2} = \left[\begin{array}{c} [(a_R/a_V)\boldsymbol{P} + \boldsymbol{Q}]^T \cdot \mathbf{1}_f \sin\beta \\ \boldsymbol{P}^T\mathbf{1}_R - (R/V)\boldsymbol{Q}^T\cdot\mathbf{1}_V \\ \boldsymbol{P}^T\cdot\mathbf{1}_V - V \end{array}\right]_{t=t_f} \tag{18}$$

For the free attachment point case we have

$$\psi_{1V} = a_v \cdot \mathbf{1}_f \tag{19a}$$

$$\psi_{1R} = -a_R \cdot \mathbf{1}_f \tag{19b}$$

$$\psi_{2V} = \mathbf{1}_V \cdot c2VV - \boldsymbol{R}\times(\boldsymbol{R}\times\boldsymbol{V})\cdot c2VR \tag{19c}$$

$$\psi_{2R} = \mathbf{1}_R \cdot c2RR - \boldsymbol{V}\times(\boldsymbol{V}\times\boldsymbol{R})\cdot c2RV \tag{19d}$$

$$\psi_{3V} = \psi_{3R} = 0 \tag{19e}$$

where

$$\begin{aligned} c2RR &= [2\cdot a^2\cdot(1-e)]/R^2 - a\cdot h^2/(R^2\cdot e) \\ c2RV &= c2VR = 1/e \\ c2VV &= 2\cdot a^2\cdot V\cdot(1-e) - a\cdot V\cdot h^2/e \\ h &= |\boldsymbol{R}\times\boldsymbol{V}|, \qquad 1/a = 2/R - V^2, \qquad e = \sqrt{1-h^2/a} \end{aligned} \tag{20}$$

The remaining terminal constraints can be obtained by building the inner product of Eq. (16) with the vectors $\mathbf{1}_f$, $(\mathbf{1}_R + \mathbf{1}_V)$, $\mathbf{1}_R$, and $\mathbf{1}_V$:

$$\psi_{\text{free},2} = \left[\begin{array}{c} [(a_R/a_V)\boldsymbol{P} + \boldsymbol{Q}]^T\cdot\mathbf{1}_f\sin\beta \\ \boldsymbol{P}^T\mathbf{1}_V - V - \tilde{\nu}_2 R^2\{c2VVe - (1/a^2)[\boldsymbol{R}\times(\boldsymbol{R}\times\boldsymbol{V})]^T\mathbf{1}_V\} \\ \boldsymbol{Q}^T\mathbf{1}_V - (1/R^2)\mathbf{1}_R^T\mathbf{1}_V - \tilde{\nu}_2\mathbf{1}_R^T\mathbf{1}_V c2RRe \\ \boldsymbol{P}^T\mathbf{1}_R - V\mathbf{1}_V^T\mathbf{1}_R - \tilde{\nu}_2\mathbf{1}_V^T\mathbf{1}_R c2VVe \end{array}\right] \tag{21}$$

where

$$\tilde{\nu}_2 = \frac{[\boldsymbol{Q} - (1/R^2)\mathbf{1}_R]^T(\mathbf{1}_R + \mathbf{1}_V)}{\{c2RRe\cdot\mathbf{1}_R - [R^2\cdot(2/R - V^2)^2]\cdot\boldsymbol{V}\times(\boldsymbol{V}\times\boldsymbol{R})\}^T\cdot(\mathbf{1}_R+\mathbf{1}_V)} \tag{22a}$$

$$c2RRe = 2\cdot(1-e)\cdot e - h^2/a \tag{22b}$$

$$c2VVe = 2\cdot V\cdot(1-e)\cdot e - V\cdot h^2/a \tag{22c}$$

Details regarding the derivations of these expressions can be found in Ref. 7.

For equatorial orbits, the first equation in $\psi_{\text{perigee},2}$ and $\psi_{\text{free},2}$ has an indefinite expression, a_R/a_V. This can be avoided by replacing the inclination constraint, as well as its associated transversality condition, by the two constraints $\mathbf{1}_N^T \cdot \boldsymbol{R}$ and $\mathbf{1}_N^T \cdot \boldsymbol{V}$. This also suggests a good method to use when the longitude of ascending node is to be constrained. In this case $\mathbf{1}_N^T \cdot \boldsymbol{R}$ and $\mathbf{1}_N^T \cdot \boldsymbol{V}$ simply need to be replaced by $\mathbf{1}_{f,d}^T \cdot \boldsymbol{R}$ and $\mathbf{1}_{f,d}^T \cdot \boldsymbol{V}$, where $\mathbf{1}_{f,d}$ is a unity vector perpendicular to the desired target orbit plane.

For circular orbits, the problem formulation for free attachment becomes singular. The denominator in Eq. (22a) is zero, and Eqs. (19c) and (19d) become indefinite. Therefore, for orbits with low eccentricity, the terminal constraints for an attachment at perigee are used. Problems similar to those described here for circular and equatorial orbits have also been described elsewhere.[8]

A Newton method is used to solve the two-point boundary value problem. Therefore, the sensitivity matrix of final states with respect to the initial costates is required. This matrix is calculated in an analytic form, except for the thrust integrals. The equations needed are presented in Ref. 1 for attachment at perigee and in Ref. 7 for the free attachment point case.

Full Optimality Condition

In a vacuum, the optimality condition reduces to $\mathbf{1}_b = \mathbf{1}_P$, which is a well-known result in the classical literature on spacecraft trajectory optimization. For the atmospheric part of the trajectory, the control dependant part of the Hamiltonian can be expressed as

$$H(\mathbf{1}_b) = P/m \cdot \left\{(T - A) \cdot \mathbf{1}_P^T \cdot \mathbf{1}_b + N \cdot \mathbf{1}_P^T \cdot \mathbf{1}_n\right\} + \text{const} \quad (23)$$

With reference to Fig. 2, the inner products can be replaced by the expressions

$$\mathbf{1}_P^T \cdot \mathbf{1}_b = \cos\delta, \qquad \mathbf{1}_P^T \cdot \mathbf{1}_n = \sin\delta, \qquad \text{where} \quad \alpha = \phi - \delta \quad (24)$$

Therefore, the optimality condition reduces to maximizing Eq. (23) with respect to α. A maximum occurs only when the body axis is lying in the plane defined by primer vector ($\mathbf{1}_p$) and the relative velocity vector ($\mathbf{1}_{V,\text{rel}}$). The first-order necessary condition $\partial H/\partial\alpha$ leads to the expression for the optimal value of δ:

$$\delta^* = \arctan\frac{N + A_\alpha}{T - A + N_\alpha} \quad (25)$$

Taking projections of the body axis on primer and relative velocity vector such that

$$\mathbf{1}_b = a_1 \cdot \mathbf{1}_p + b_1 \cdot \mathbf{1}_{V,\text{rel}} \quad (26)$$

a_1 and b_1 can be calculated as

$$b_1 = \frac{\cos\alpha^* - \cos\delta^* \cdot \cos\phi}{\sin^2\phi}, \qquad a_1 = \cos\delta^* - b_1 \cdot \cos\phi \quad (27)$$

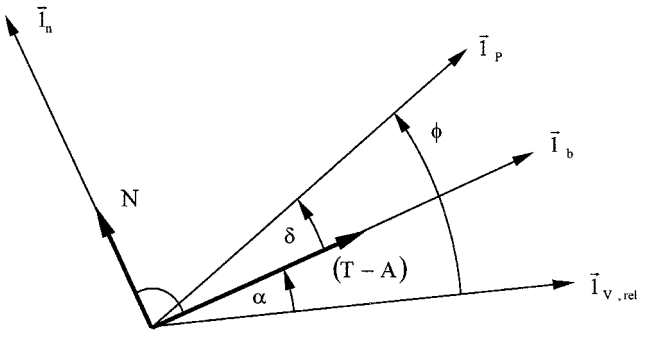

Fig. 2 Optimal control within atmosphere.

Path Constraints

In Ref. 1, an axial acceleration limit is approximated by the condition $T_{\text{vac}}/m \le a_{\max}$. This approximation assumes that thrust is always dominating over other specific forces, which is perfectly valid outside the atmosphere. Within the atmosphere, the approximation is conservative and assures that axial acceleration is asymptotically approaching its limit. The axial acceleration limit is enforced in the optimization process by regulating the mass flow. The necessary conditions for enforcing normal force and angle-of-attack limits are summarized in this section.

For a normal force limit, the constraint

$$|N(\alpha)| \le N_{\max} \quad (28)$$

has to be satisfied. If the condition in Eq. (25) results in a violation of this constraint, the angle of attack α is calculated from the condition

$$N(\alpha') = N_{\max} \quad (29)$$

The constraint multiplier ε_N is then calculated such that

$$\frac{\partial H}{\partial\alpha} = \left\{\frac{|\boldsymbol{P}|}{m}[\sin(\phi - \alpha) \cdot (T - A + N_\alpha) - \cos(\phi - \alpha) \cdot (N + A_\alpha)] + \varepsilon_N \cdot N_\alpha\right\}_{\alpha=\alpha'} = 0 \quad (30)$$

The similar procedure applies for the angle of attack constraint. When either constraint is active, the corresponding constraint multipliers are used to modify the expressions for the costate collocation variables in Eq. (9) according to

$$\boldsymbol{q}_V(t) = -\frac{\partial H_{\text{atmos}}}{\partial \boldsymbol{V}} - \varepsilon_N \cdot \frac{\partial N}{\partial \boldsymbol{V}} - \varepsilon_\alpha \cdot \frac{\partial \alpha}{\partial \boldsymbol{V}}$$
$$\boldsymbol{q}_R(t) = \frac{\partial H_{\text{atmos}}}{\partial \boldsymbol{R}} + \varepsilon_N \cdot \frac{\partial N}{\partial \boldsymbol{R}} + \varepsilon_\alpha \cdot \frac{\partial \alpha}{\partial \boldsymbol{R}} \quad (31)$$

If both constraints are violated, the constraint resulting in the smaller angle of attack is enforced, and the constraint multiplier for the other constraint is set to zero.

Optimizing Coast Arcs

When using the method of collocation, the time interval must be divided into sufficiently short elements defined by a set of nodal times. Since coast arcs are handled completely analytically, additional nodes for coast arcs are not required. Coast arcs can be thought of as being inserted into separate stages, or subdividing a single stage into multiple burn arcs. When coast arcs are used to separate a stage, only the duration of the coast arc is optimized. When coast arcs are used to subdivide a single stage, then both, the start and the end of each coast arc, are optimized, recognizing that the total burn time of a stage is fixed. For this study, a method similar to that suggested in Ref. 9 was employed.

To optimize a coast arc in time, a switching function similar to that used in Refs. 4 and 5 can be defined as

$$S(t) = |\boldsymbol{P}|/m - \lambda_m/c_e \quad (32)$$

Since H is constant over burn and coast arcs whenever the optimality condition is satisfied, Eq. (32) can be rewritten as

$$S = 1/T_{\text{vac}} \cdot (H - \boldsymbol{Q}^T \cdot \boldsymbol{V} + \boldsymbol{P}^T \cdot \boldsymbol{R}/R^3) \quad (33)$$

where H is the value of the Hamiltonian in the current burn arc. The Hamiltonian at final time can be calculated using the fact that, because neither the performance index nor any of the terminal

constraints depend on mass, the costate λ_m is zero at final time. The Hamiltonian can then be expressed as

$$H(t_f) = \boldsymbol{P}_f^T \cdot \left(-\boldsymbol{R}_f \Big/ R_f^3 + T_{\text{vac}}/m \cdot \mathbf{1}_{p,f}\right) + \boldsymbol{Q}_f^T \cdot \boldsymbol{V}_f \qquad (34)$$

In general, H is discontinuous between a burn and a coast arc as long as the coast arc is not optimal. Hence, during the optimization process, H in Eq. (33) has to be the value of H for the specific burn arc over which the solution is being integrated. To calculate this value, the facts that H is constant within a burn arc and λ_m is constant within a coast arc (and continuous at the switching points between burn and coast arcs) are used. The value for $S(t)$ can then be calculated backward in time. For the optimization, only the values of $S(t)$ at the start and end points of a burn arc are required.

The condition

$$\delta J = H(t_f) \cdot \mathrm{d}t_f + \int_{t_0}^{t_f} H_u(x, \lambda, u, t)\delta u \, \mathrm{d}t \le 0 \qquad (35)$$

has to be satisfied for the optimal position and duration of a coast arc. In this study, coast arcs are assumed to occur only within the last stage of the vehicle. Thrust is assumed constant within this stage (since the last stage thrust/weight ratio is very low, axial acceleration limits are never exceeded). If small variations are considered at the start and end times of the coast arc, as shown in Fig. 3, and burn time is kept constant by the condition

$$(t_2 - t_1) + \cdots + (t_{2n} - t_{2n-1}) = (t_2 + \delta t_2 - t_1) + \cdots + (t_{2n} + \delta t_{2n} - t_{2n-1} - \delta t_{2n-1})$$

$$\delta t_{2n} = \delta t_3 + \delta t_5 + \cdots + \delta t_{2n-1} - \delta t_2 - \delta t_4 - \cdots - \delta t_{2n-2} \qquad (36)$$

then Eq. (35) can be written as

$$\delta J = \delta t_2 \cdot [T \cdot S(t_2) - H_f] + \delta t_3 \cdot [H_f - T \cdot S(t_3)] + \cdots + \delta t_{2n-2} \cdot [S(t_{2n-2}) \cdot T - H_f] + \delta t_{2n-1} \times [H_f - T \cdot S(t_{2n-1})] \le 0 \qquad (37)$$

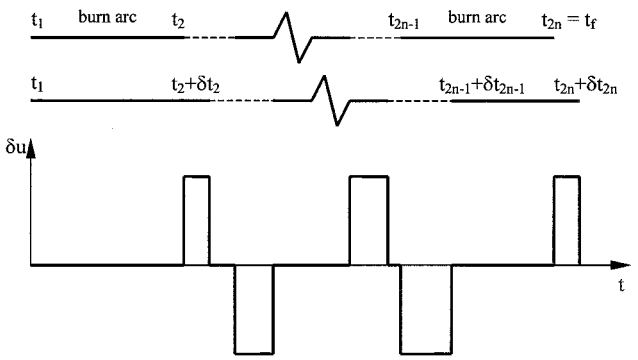

Fig. 3 Adjusting coast arc start and end points.

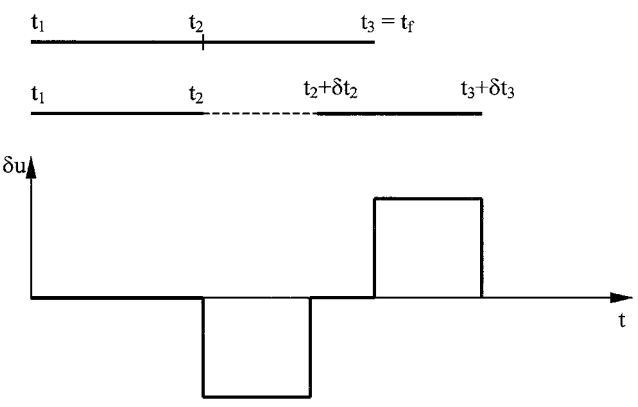

Fig. 4 Inserting additional coast arc.

Since Eq. (37) must hold for any arbitrary δt_i, the necessary conditions for optimality become

$$S(t_2) = S(t_3) = \cdots = S(t_{2n-2}) = S(t_{2n-1}) = H_f/T \qquad (38)$$

Defining

$$\begin{aligned} \Delta S_a &= S_2 - S_3 \\ \Delta S_b &= S_3 - S_4 \\ &\vdots \\ \Delta S_z &= S_{2n-2} - S_{2n-1} \\ \Delta F &= S_{2n-1} - H_f/T \end{aligned} \qquad (39)$$

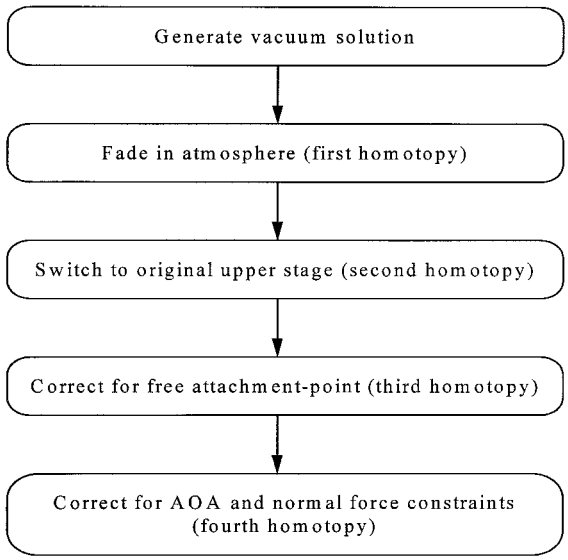

Fig. 5 Summary of solution method.

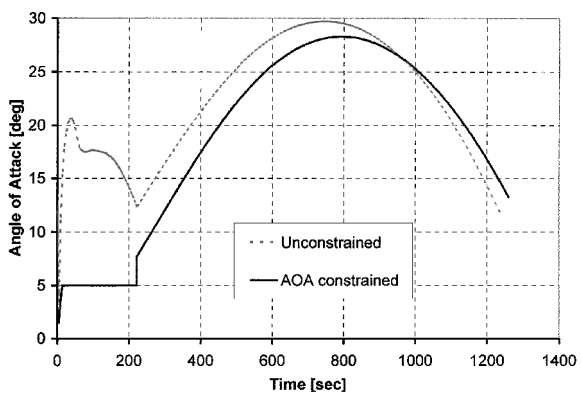

Fig. 6 Constrained angle of attack.

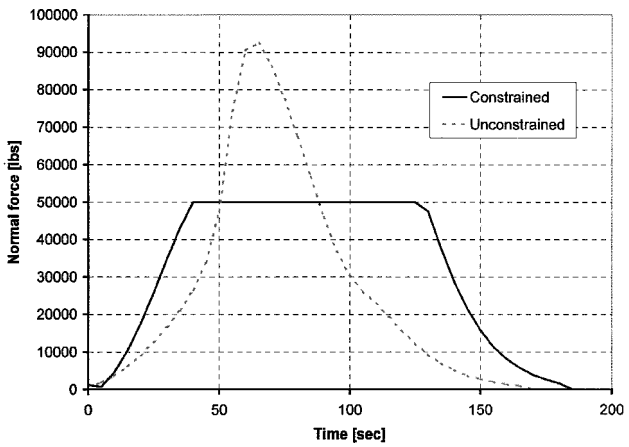

Fig. 7 Constrained normal force.

and considering small variations in the switching times, we have

$$\begin{aligned}
\delta\Delta S_a &= \dot{S}_2\delta t_2 - \dot{S}_3\delta t_3 \\
\delta\Delta S_b &= \dot{S}_3\delta t_3 - \dot{S}_4\delta t_4 \\
&\vdots \\
\delta\Delta S_z &= \dot{S}_{2n-2}\delta t_{2n-2} - \dot{S}_{2n-1}\delta t_{2n-1} \\
\delta\Delta F &= \dot{S}_{2n-1}\delta t_{2n-1}
\end{aligned} \tag{40}$$

Setting the error terms in Eq. (40) to zero results in a system of linear equations

$$\begin{bmatrix}
\dot{S}_2 & -\dot{S}_3 & & & 0 \\
 & \dot{S}_3 & -\dot{S}_4 & & \\
 & & \ddots & & \\
 & & & \dot{S}_{2n-2} & -\dot{S}_{2n-1} \\
0 & & & & \dot{S}_{2n-1}
\end{bmatrix} \cdot \begin{bmatrix} \delta t_2 \\ \delta t_3 \\ \vdots \\ \delta t_{2n-2} \\ \delta t_{2n-1} \end{bmatrix} = \begin{bmatrix} -\Delta S_a \\ -\Delta S_b \\ \vdots \\ -\Delta S_z \\ -\Delta F \end{bmatrix} \tag{41}$$

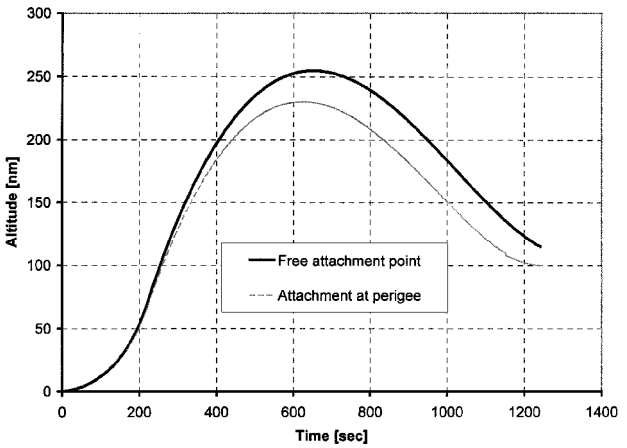

Fig. 8 Free vs perigee attachment.

where it can be shown that

$$\dot{S} = -\boldsymbol{P}^T \cdot \boldsymbol{Q}/(|\boldsymbol{P}| \cdot m) \tag{42}$$

From Eq. (41), it follows that to first order, the variation in the switching times needed to attain the optimality conditions in Eq. (38) are

$$\delta t_i = (H_f/T - S_i)/\dot{S}_i \tag{43}$$

Note that the necessary conditions in Eq. (38) do not impose any condition on the value of the switching function at the final time. The absence of imposed conditions is due to the fact that the conditions are derived for the situation where the number of coast arcs is defined a priori. In fact, it is possible to use the value of $S(t_f)$ to determine if the number of coast arcs is optimal. Optimality can be concluded by considering Fig. 4, which illustrates a portion of the final burn arc. Consider the situation in which $S(t_f) < H_f/T$. If an additional coast arc is inserted at time t_2, where $S(t_2)$ is still $< H_f/T$, then from Eq. (35) the resulting change in the performance index would be

$$\delta J = [H_f - T \cdot S(t_2)] \cdot \delta t_2 > 0 \tag{44}$$

Therefore, a solution involving an additional coast arc would increase the performance. The reverse can be argued when $S(t_f) < H_f/T$.

Summary of the Solution Method

Figure 5 illustrates a summary of the solution method. First, a vacuum solution is generated using the terminal constraints for perigee attachment. It was observed that for the case of a low thrust/weight upper stage, the vacuum solution initially passes below the Earth's surface. This presents a problem when the atmospheric terms are introduced using the method of collocation. If this occurs, the upper stage trust is increased. After the vacuum solution is generated, atmospheric effects are introduced in a first homotopy phase as described in Ref. 1, after which the original vehicle data is restored (if needed) in a second homotopy phase. After this, the attachment point to the final orbit is also optimized by switching the terminal constraints and correcting the collocation parameters in a third homotopy. Finally, angle of attack and normal force limits are enforced during a fourth homotopy phase.

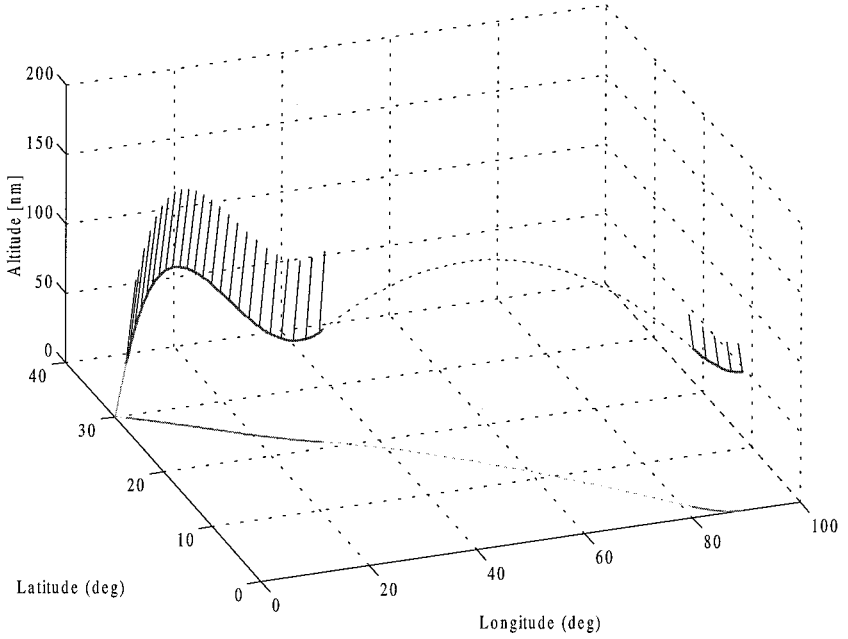

Fig. 9 Ascent trajectory with coast arc.

For elliptical orbits, a solution with attachment at perigee is generated first. Once the atmosphere is partly faded in, the terminal constraints are switched to the more general set for a free attachment point. This procedure is faster than using free attachment point constraints from the very beginning.

Optimal ascent trajectories into orbits not involving coast arcs can be generated completely automatically within 10–15 min on a Pentium II 400 MHz system using MATLAB®, starting with an arbitrary initial guess for the costate vector. When coded in C^{++}, the execution time is reduced by approximately a factor of 10. For real time applications, where a good starting guess is provided, a guidance update can be calculated in fractions of a second.[1]

Numerical Results

In this section, we present results from several cases to highlight the characteristics of the resulting ascent profiles. The vehicle data and a more complete description of the boundary conditions for all the cases can be found in Appendix Tables A1–A3 and Ref. 7. Figure 6 illustrates an optimal angle of attack profile for a vehicle with a low thrust/weight ratio in the upper stage. The dashed line corresponds to an unconstrained profile, whereas the solid line is a result obtained when the angle of attack was constrained to be a maximum of 5 deg in the first stage. Total burn time for the constrained ascent is increased by about 18.6 s. Figure 7 illustrates the normal force profile result for the same vehicle with a normal force limit. The dashed line is, again, the unconstrained profile. The solid line corresponds to an ascent with a normal force constraint of 50,000 lbs (222.4 kN). Total burn time for the constrained ascent is about 7 s longer.

For vehicles with a low thrust/weight ratio upper stage, the difference between attachment at perigee and a free attachment point solution is much more significant than that observed for conventional vehicles. Figure 8 shows a comparison of the altitude profiles for a case in which the target orbit is elliptical, with an eccentricity of 0.188. The perigee radius is 100 nm and the attachment point has a true anomaly of 13.4 deg. Burning time for the free attachment point solution is 6 s shorter than for attachment at perigee. This difference in burn time is equivalent to a mass difference of 555 lb (251.7 kg).

Figure 9 illustrates an optimized ascent into a 100-nm circular equatorial orbit from 30-deg launch latitude. The vehicle data are shown in the Appendix. This ascent involves a coast arc, starting at 834.8 s, with a duration of 845.5 s. Figure 10 gives the profile of the switching function in the upper part of the trajectory. It can be seen clearly that the burn arcs are ending just when the triggering value H_f/T is reached. This case has been validated by comparing

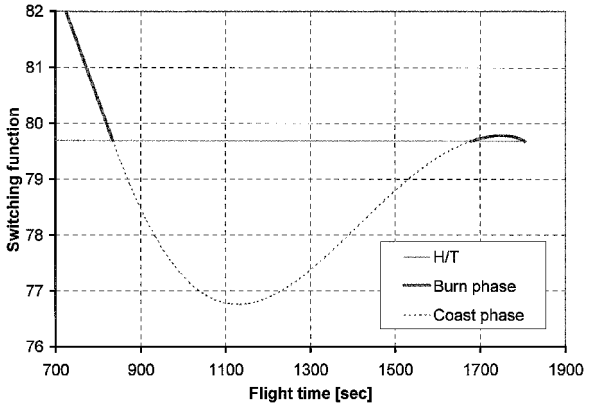

Fig. 10 Switching function for ascent to a circular equatorial orbit.

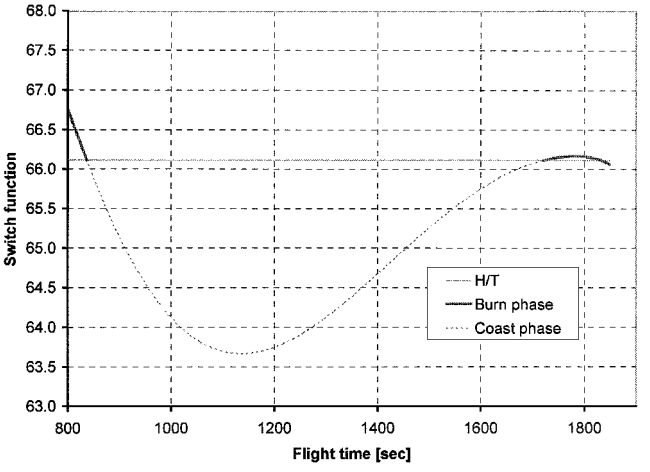

Fig. 12 Switching function for ascent to elliptical orbit.

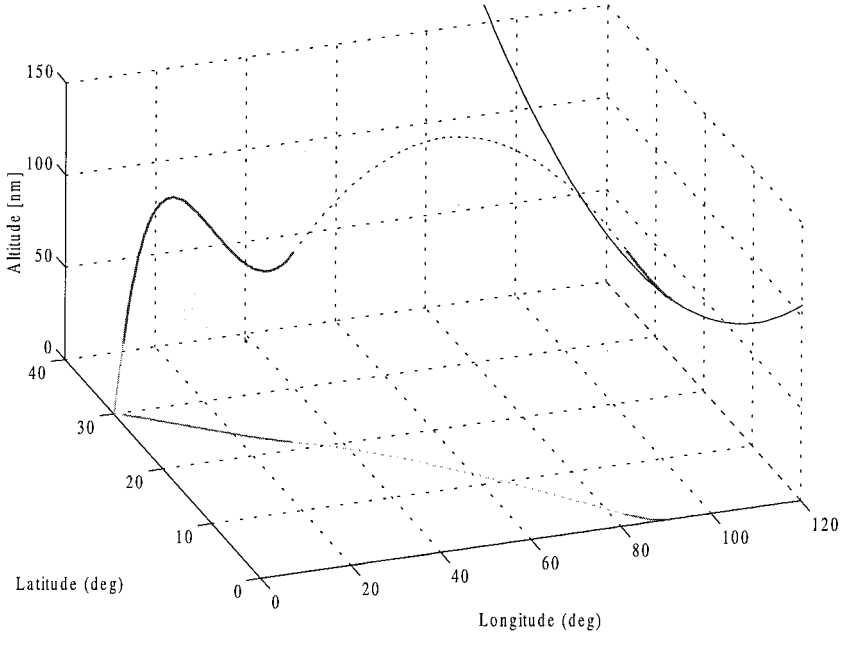

Fig. 11 Ascent to an elliptical orbit with only one coast arc.

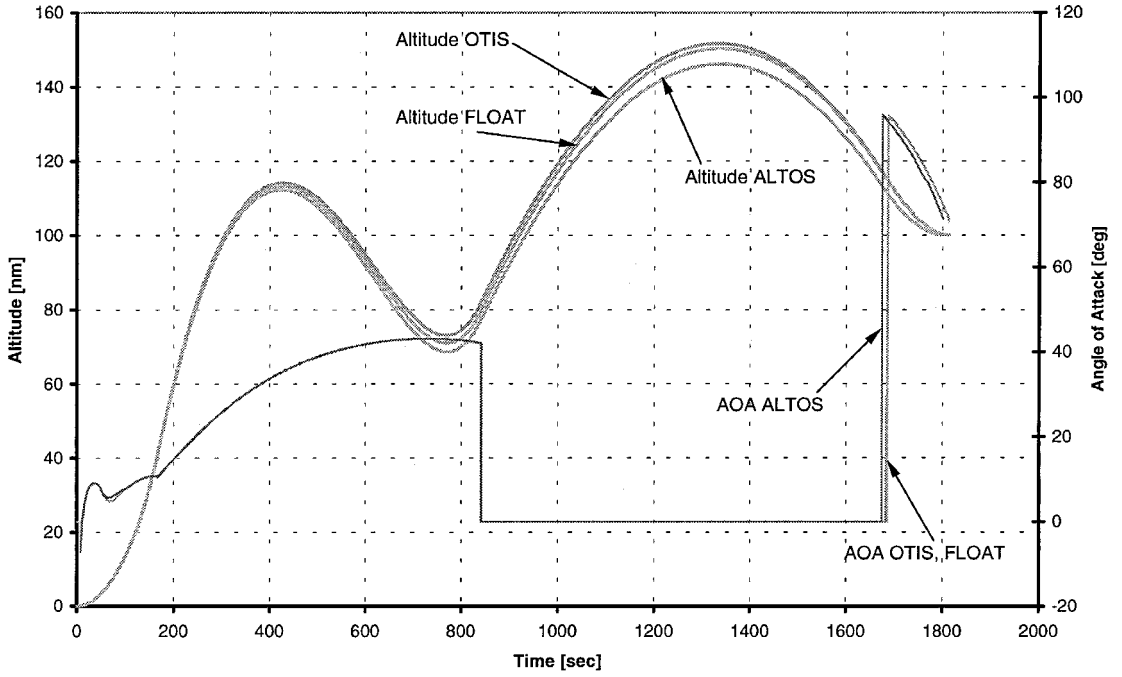

Fig. 13 Comparison with OTIS and ALTOS.

it with independent optimization codes as mentioned below. The optimal solution with one coast arc is shown in Fig. 11 for the case where the circular orbit is changed to an elliptical orbit with apogee at 1000 nm altitude. For this case, executing the total inclination change at perigee is not optimal. Instead, a third burn in apogee would further reduce fuel consumption. This can be concluded from Eq. (44) by noting that the plot of the switching function in Fig. 12 falls below H_f/T during the last few seconds of the second burn.

Figure 13 shows a comparison of the results of three different trajectory optimization codes for the mission to a 100 nm circular equatorial orbit described above. Fast Logic for Optimization of Ascent Trajectories (FLOAT) is the code presented in this paper. Optimal Trajectories by Implicit Simulation (OTIS)[10] and Advanced Launcher Trajectory Optimization Software (ALTOS)[11] are two different direct optimization methods using control discretization. The small deviations are likely due to the differences in the way the atmospheric model and the optimal solution are parameterized in these approaches.

Conclusions

A variety of improvements to a previously developed hybrid optimization code has been described. These improvements are aimed at making the resulting code more applicable to both vehicle design and, ultimately, real time guidance of advanced launch vehicle configurations. In particular, it was found that reducing the thrust/weight ratio of the upper stage has a dramatic effect on the angle of attack profile, both in the atmospheric and exoatmospheric flight phases. Therefore, simultaneous guidance optimization of both flight phases will play an important role in attaining optimum system performance and can significantly impact the overall vehicle design as well. Furthermore, the performance difference between attaching at perigee and free attachment is increased. The implication from a synthesis perspective is that the boundary conditions for free attachment are considerably more complicated to enforce than the boundary conditions for attachment at perigee.

For cases involving coast arcs, the solution process requires the number of coast arcs to be predefined for each burn stage. However, a method for determining when the number of coast arcs is optimal is also provided as a by-product of the solution. Unfortunately, optimal ascents with coast arcs can take considerably longer to converge. This longer computation time is due to the fact that there is a strong coupling between the atmospheric portion of the solution and the location of the coast arcs.

Appendix: Example Vehicle Data

Table A1 Axial force coefficient

M	Axial force coefficient
0	0.35
0.6	0.35
0.8	0.37
0.9	0.41
0.95	0.45
1.0	0.50
1.05	0.59
1.1	0.68
1.2	0.77
1.4	0.76
1.6	0.70
1.97	0.58
2.48	0.45
2.97	0.48
≥4	0.54

Table A2 Normal force coefficient

α	Normal force coefficient
−20	−1
−15	−0.75
−10	−0.5
−5	−0.25
0	0
5	0.25
10	0.5
15	0.75
20	1

Table A3 Vehicle stage properties[a]

Property	Stage 1	Stage 2
A_{ref}	135 ft^2 (12.54 m^2)	135 ft^2 (12.54 m^2)
m_f	107,678.04 lb (48,842 kg)	maximized
m_{drop}	24,678.45 lb (11,194 kg)	0 lb (0 kg)
T_{vac}	432,500 lb (1,923.9 kN)	41,500 lbs (184,6 kN)
A_e	20.7 ft^2 (1.923 m^2)	26.2 ft^2 (2.434 m^2)
ISP	443 s	456 s

[a]Initial mass = 263,298.53 lb (119,430 kg); and launch latitude = 30°.

Acknowledgment

This research has been supported by the Boeing Company, Space Systems, Huntington Beach, California.

References

[1]Calise, A. J., Melamed, N., and Lee, S., "Design and Evaluation of a Three-Dimensional Optimal Ascent Guidance Algorithm," *Journal of Guidance, Control, and Dynamics*, Vol. 21, No. 6, 1998, pp. 867–875.

[2]Goodyear, W. H., "Completely General Closed-Form Solution for Coordinates and Partial Derivatives of the Two-Body Problem," *Astronomical Journal*, Vol. 70, No. 3, 1965, pp. 189–192.

[3]Brown, K. R., Harrold, E. F., and Johnson, G. W., "Rapid Optimization of Multiple-Burn Rocket Flights," NASA CR-1430, Sept. 1969.

[4]Jezewski, D. J., "Optimal Analytic Multiburn Trajectories," *AIAA Journal*, Vol. 10, No. 5, 1972, pp. 680–685.

[5]McAdoo, S. F., Jezewski, D. J., and Dawkins, G. S., "Development of a Method for Optimal Maneuver Analysis of Complex Space Missions," NASA TN D-7882, April 1975.

[6]Jezewski, D. J., "OMEGA: An Approximate Analytic Solution of N-Burn Optimal Trajectories," NASA Manned Spacecraft Center, Internal Note 72-FM-232, Houston, TX, Sept. 1972.

[7]Gath, P. F., "Improvements to a Hybrid Algorithm for Rapid Generation of 3-D Optimal Launch Vehicle Ascent Trajectories," Diploma Thesis, IFR_SR_98_016, Inst. of Flight Mechanics and Control, Univ. of Stuttgart, Stuttgart, Germany, Dec. 1998, Chap. 2.

[8]Brown, K. R., and Johnson, G. W., "Real-Time Optimal Guidance," *IEEE Transactions on Automatic Control*, Vol. AC-12, No. 5, 1967, pp. 501–506.

[9]Calise, A. J., and Nagy, J., "Necessary Conditions for Optimal Pulse Control," *Journal of Guidance, Control, and Dynamics*, Vol. 9, No. 1, 1986, pp. 53–57.

[10]Vlases, W. G., et al., "Optimal Trajectories by Implicit Simulation, Version 2, User's Manual," WRDC-TR-90-3056, Dec. 1990.

[11]Well, K. H., Markl, A., and Mehlem, K., "ALTOS: A Software Package for Simulation and Optimization of Trajectories of Launch and Reentry Vehicles," *Proceedings of the 48th International Astronautical Congress*, IAF-97-V4.04, Turin, Italy, Oct. 1997.